Diode Open-Circuit Fault Research on the Parallel-Connected 36-Pulse Rectifier With Dual Passive Harmonic Reduction Method

Qingxiao Du, Lei Gao, Quanhui Li, Xinyu Yin, and Fangang Meng, *Member, IEEE*

***Abstract*—To clarify the influence of using different harmonic reduction circuits (HRCs) on open-circuit fault characteristics, and the relationship between steady-state and fault-state power quality of the multi-pulse rectifiers (MPRs), this article focuses on the diode open-circuit fault research of the parallel-connected 36-pulse rectifier with dc-side dual passive HRC. Based on the normal operation modes of the MPR, the fault characteristics under diode open-circuit fault in the main circuit and the HRC are discussed in detail. Besides, the power quality comparisons between the MPRs with single or dual passive HRC are presented under fault conditions. From the simulation and experiment verification results, the load voltage can exactly reflect the location of the fault diode, and fault diode located in the dc-side HRC causes less damage on the power quality of the MPR. In general, compared with single passive HRC, dual passive HRC can reduce the impact of diode open-circuit fault on ac-side power quality. Adding dual passive HRC is a reliable method to improve the power quality of MPRs.**

***Index Terms*—36-pulse rectifier, dc-side dual-passive harmonic reduction method, diode open-circuit fault research.**

I. Introduction

With development of power electronic technology, rectifiers, as one of the most commonly used power electronic devices, have been widely used in power systems, industrial and agricultural production, transportation, and household electricity. Meanwhile, the problem of harmonic pollution caused by the strong nonlinearity of power electronic devices has become more and more serious. Harmonic pollution has become the main barrier restricting the development of power electronic technology. Multipulse rectification technology is one of effective technologies that can deal with harmonics.

Manuscript received September 17, 2021; revised November 7, 2021; accepted December 20, 2021. Date of publication December 23, 2021; date of current version February 18, 2022. This work was supported in part by the National Natural Foundation of China under Grant 51777042, in part by the China Scholarship Council, and in part by the CSC Grant for Qingxiao Du's Scholarship of Research Visiting at Aalborg University, Denmark. Recommended for publication by Associate Editor N. Zargari. *(Corresponding author: Fangang Meng.)*

The authors are with the School of Electrical Engineering and Automation, Harbin Institute of Technology, Harbin 150001, China (e-mail: 690384469@qq.com; hualeier111@126.com; a875921420@qq.com; yxy06281205@163.com; mfg0327@sina.com).

Color versions of one or more figures in this article are available at https://doi.org/10.1109/TPEL.2021.3137894.

Digital Object Identifier 10.1109/TPEL.2021.3137894

Multipulse rectifiers (MPRs) have the advantages of easy implementation, high reliability, strong overload capacity, and low overall cost, so that they are widely used in some industrial fields, such as the HVdc transmission, uninterruptable power system, and aircraft converter system [1]. In the early development stage of multipulse rectification technology, researchers increased the number of three-phase bridge rectifiers in the main circuit to increase the number of pulses and reduce the harmonic content [2], [3]. Although this method has a simple harmonic reduction mechanism and is easy to design, in order to achieve a good harmonic elimination effect, it is necessary to use more complicated phase-shifting transformers, interphase reactors (IPRs), and other magnetic components. In the past two decades, the research on dc-side harmonic reduction methods have become the focus of attention [4]–[13]. Depend on the device type in the harmonic reduction circuits (HRCs), they can be divided into the passive, active, and hybrid harmonic reduction methods. Compared with the HRCs using active devices, the passive HRCs do not need control and drive circuit, the reliability has been improved to some extent, and this article is mainly focused on MPRs with passive HRC. Among them, the most common HRCs are often combined with the 12-pulse rectifier. When the conventional 12-pulse rectifier combines with the single or dual passive HRC, the 24- or 36-pulse rectifiers can be formed [7]–[10]. Under steady-state conditions, the theoretical THD values of the 24- or 36-pulse rectifiers are $\sim$7.55% and $\sim$5.04%, respectively. Previous studies have shown that using dc-side dual passive HRC is an effective way to further improve the power quality of the MPRs, so as to better meet the requirements of most industries for harmonic content.

In addition to normal operation mode, the operating characteristics and power quality of the MPR under fault conditions are also important factors to evaluate the overall performance. Generally, when short-circuit fault occurs, the relay protection device will timely operate and cutoff the fault due to the overcurrent. Under open-circuit conditions, although MPRs can keep working for a certain time, during this period, the power quality is inevitably affected. It should be noted that research on open-circuit fault characteristic is an essential precondition for fault detecting. In [14], the open-phase fault at the primary side of the phase-shifting transformer is studied, and Perisé *et al.* [15] are mainly focusing on diode open-circuit of MPRs without any HRC. Recently, the diode open-circuit fault research

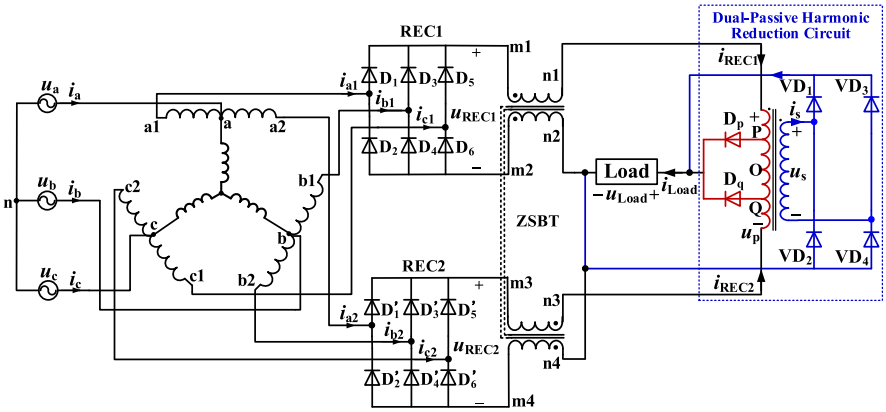

Fig. 1. Parallel-connected 36-pulse rectifier.

for the 24-pulse rectifier with single passive HRC has been presented in [16], however, whether the fault tolerance ability of the 36-pulse rectifier can also be improved remains to be studied. The magnetic devices, such as the phase-shifting transformer and IPR, are also an important part of the MPR. In actual, the internal failure on the magnetic devices is a process of gradual accumulation, so that the probability of this failure is lower than the diode failure. For typical external faults of magnetic devices, such as an open-circuit fault on the secondary-side transmission line, it can be equivalent to diodes open-circuit fault in the main circuit. Therefore, the research on the diode open-circuit fault is the basis and focus of the fault tolerance research.

In order to find the relations between the power quality of MPRs under steady-state and fault conditions, explore the impact of the HRCs on the fault tolerance performance of the MPRs. On the basis of the steady-state operation modes, this article will discuss the fault characteristic of the 36-pulse rectifier under diode open-circuit faults both in the main circuit and the dc-side HRC. Under the same fault condition, the ac and dc sides power quality will be compared between the 24- and 36-pulse rectifiers. This article aims to provide theoretical guidance for fault detection and future MPR design.

II. Normal Operation Mode Analysis on the Parallel-Connected 36-Pulse Rectifier

This section establishes the voltage relations between ac and dc sides of the 36-pulse rectifier, the related voltage waveforms under normal operation mode are plotted, which can provide foundations and references for fault analysis.

Fig. 1 is the parallel-connected 36-pulse rectifier with dc-side dual-passive HRC. The zero-sequence blocking transformer is used to absorb the zero-sequence current and ensure that the rectifier with the Y-connected autotransformer can operate normally. The primary and secondary sides of the IPR are connected with two diodes and a single-phase diode bridge rectifier, respectively. Due to that, this article is the further fault research of the rectifier presented in [10], the detailed information of the rectifier in Fig. 1 is omitted here to avoid repetition.

The formation process of the 36-pulse rectifier is the combination effect of the dc-side single-phase rectifier and the 24-pulse rectifier with the double-tap IPR. In the following derivations, the values associated with the 12, 24, and 36 pulse rectification states are, respectively, marked with the subscript "12," "'24," and "36."

Defining that the turns ratios α_m and m of the IPR are as follows:

$$\begin{cases} \alpha_{\rm m} = N_{\rm PO(OQ)}/N_0 \\ m = N_{\rm s}/N_0 = u_{\rm s}/u_{\rm p} \end{cases} \tag{1}$$

where point "O" is the midpoint of the primary side winding, points "P" and "Q" are the two points connected with the two diodes in the primary side, N_0 is the overall primary side winding number; and $N_{\rm s}$ is the number of the secondary side winding.

Assuming that the three-phase input voltages of the MPR are as follows:

$$\begin{cases} u_{\rm a} = \sqrt{2}E\sin\omega t \\ u_{\rm b} = \sqrt{2}E\sin(\omega t - 2\pi/3) \\ u_{\rm c} = \sqrt{2}E\sin(\omega t + 2\pi/3) \end{cases} \tag{2}$$

where E is the rms value of the input voltage.

The six-phase output voltages of the Y-connected phase-shifting transformer are as follows:

$$\begin{cases} u_{\rm a1} = \sqrt{2}KE\sin(\omega t + \pi/12) \\ u_{\rm b1} = \sqrt{2}KE\sin(\omega t - 7\pi/12) \\ u_{\rm c1} = \sqrt{2}KE\sin(\omega t + 3\pi/4) \\ u_{\rm a2} = \sqrt{2}KE\sin(\omega t - \pi/12) \\ u_{\rm b2} = \sqrt{2}KE\sin(\omega t - 3\pi/4) \\ u_{\rm c2} = \sqrt{2}KE\sin(\omega t + 7\pi/12) \end{cases} \tag{3}$$

where K is the step-up ratio of the transformer.

If only using the double-tap IPR, the operation modes of the three-phase rectifiers REC1 and REC2 are still in the 12-pulse rectification state, so that the output voltages of rectifiers REC1 and REC2 are as follows:

$$\begin{cases} u_{\rm REC1\_24} = u_{\rm REC1\_12} = S_{\rm a1\_12}u_{\rm a1} + S_{\rm b1\_12}u_{\rm b1} + S_{\rm c1\_12}u_{\rm c1} \\ u_{\rm REC2\_24} = u_{\rm REC2\_12} = S_{\rm a2\_12}u_{\rm a2} + S_{\rm b2\_12}u_{\rm b2} + S_{\rm c2\_12}u_{\rm c2}. \end{cases} \tag{4}$$

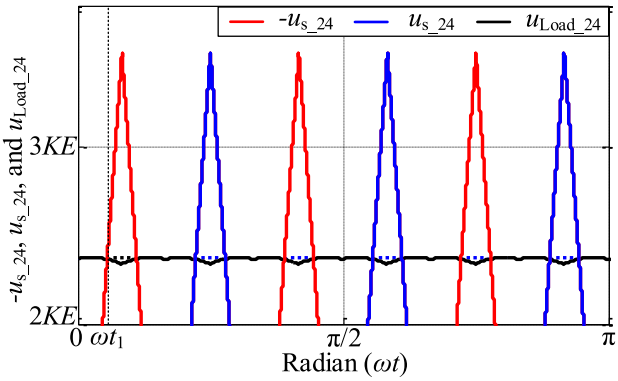

Fig. 2. Formation of the 36-pulse load voltage $u_{\mathrm{Load\_36}}$.

Based on the voltage relations in (3), the switching function of each phase can be expressed as follows:

$$\begin{cases} S_{\mathrm{a1\_12}} = 0.5\left\{\mathrm{sgn}\left[u_{\mathrm{a1}} - u_{\mathrm{b1}}\right] - \mathrm{sgn}\left[u_{\mathrm{c1}} - u_{\mathrm{a1}}\right]\right\} \\ S_{\mathrm{b1\_12}} = 0.5\left\{\mathrm{sgn}\left[u_{\mathrm{b1}} - u_{\mathrm{c1}}\right] - \mathrm{sgn}\left[u_{\mathrm{a1}} - u_{\mathrm{b1}}\right]\right\} \\ S_{\mathrm{c1\_12}} = 0.5\left\{\mathrm{sgn}\left[u_{\mathrm{c1}} - u_{\mathrm{a1}}\right] - \mathrm{sgn}\left[u_{\mathrm{b1}} - u_{\mathrm{c1}}\right]\right\} \\ S_{\mathrm{a2\_12}} = 0.5\left\{\mathrm{sgn}\left[u_{\mathrm{a2}} - u_{\mathrm{b2}}\right] - \mathrm{sgn}\left[u_{\mathrm{c2}} - u_{\mathrm{a2}}\right]\right\} \\ S_{\mathrm{b2\_12}} = 0.5\left\{\mathrm{sgn}\left[u_{\mathrm{b2}} - u_{\mathrm{c2}}\right] - \mathrm{sgn}\left[u_{\mathrm{a2}} - u_{\mathrm{b2}}\right]\right\} \\ S_{\mathrm{c2\_12}} = 0.5\left\{\mathrm{sgn}\left[u_{\mathrm{c2}} - u_{\mathrm{a2}}\right] - \mathrm{sgn}\left[u_{\mathrm{b2}} - u_{\mathrm{c2}}\right]\right\}. \end{cases} \tag{5}$$

The primary side terminal voltage of the IPR is as follows:

$$u_{\mathrm{p\_24}} = u_{\mathrm{REC1\_24}} - u_{\mathrm{REC2\_24}}. \tag{6}$$

In combination with Kirchhoff's voltage law (KVL) and (6), it can be obtained that the diodes D_p and D_q alternatively conduct. The load voltage of the 24-pulse rectifier is as follows:

$$u_{\mathrm{Load\_24}} = \begin{cases} u_{\mathrm{REC1\_24}} - (0.5 - \alpha_{\mathrm{m}})u_{\mathrm{p\_24}}u_{\mathrm{p\_24}} > 0 \\ u_{\mathrm{REC1\_24}} - (0.5 + \alpha_{\mathrm{m}})u_{\mathrm{p\_24}}u_{\mathrm{p\_24}} < 0. \end{cases} \tag{7}$$

After adding the second passive HRC on the secondary side of the IPR, the operation modes of the main circuit will change. As shown in Fig. 2, ωt_1 is the intersection point of the voltages $u_{\mathrm{s\_24}}$ and $u_{\mathrm{Load\_24}}$, there are four operation modes of the dc-side dual passive HRC.

1) *Mode 1:* $u_{s\_24}<0\&|u_{s\_24}|<u_{\mathrm{Load\_24}}$, in the intervals of $\omega t \in [2k\pi, \omega t_1 + 2k\pi) \cup [\pi/6 - \omega t_1 + 2k\pi, \pi/6 + 2k\pi)$, k is a natural number.

Under this case, the diode D_q is turned-ON, but the single-phase rectifier does not work. The output voltages of the three-phase bridge rectifiers and load voltage satisfy (4) and (7).

2) *Mode 2:* $u_{s\_24}<0\&-u_{s\_24}>u_{\mathrm{Load\_24}}$, in the interval of $\omega t \in [\omega t_1 + 2k\pi, \pi/6 - \omega t_1 + 2k\pi)$.

Under this case, the diodes D_q, VD_2, and VD_3 are turned-ON. Based on the KVL, the voltages relations are as follows:

$$\begin{cases} u_{\mathrm{REC2\_36}} + (0.5 - \alpha_{\mathrm{m}})u_{\mathrm{p\_36}} = -u_{\mathrm{s\_36}} = u_{\mathrm{Load\_36}} \\ u_{\mathrm{REC1\_36}} - u_{\mathrm{REC2\_36}} = u_{\mathrm{p\_36}} = \frac{u_{\mathrm{s\_36}}}{m} \\ u_{\mathrm{REC2\_36}} = u_{\mathrm{REC2\_24}}. \end{cases} \tag{8}$$

From (8), the voltages $u_{\mathrm{REC1\_36}}$ and $u_{\mathrm{Load\_36}}$ can be represented by the voltage $u_{\mathrm{REC2\_24}}$

$$\begin{cases} u_{\mathrm{REC1\_36}} = \frac{2m-1-2\alpha_{\mathrm{m}}}{2m+1-2\alpha_{\mathrm{m}}} u_{\mathrm{REC2\_24}} \\ u_{\mathrm{Load\_36}} = \frac{2m}{2m+1-2\alpha_{\mathrm{m}}} u_{\mathrm{REC2\_24}}. \end{cases} \tag{9}$$

3) *Mode 3:* $u_{s\_24}>0\&|u_{s\_24}|<u_{\mathrm{Load\_24}}$, in the intervals of $\omega t \in [\pi/6 + 2k\pi, \pi/6 + \omega t_1 + 2k\pi) \cup [\pi/3 - \omega t_1 + 2k\pi, \pi/3 + 2k\pi)$.

Under this case, the diode D_p is turned-ON, but the single-phase rectifier does not work. The output voltages of the three-phase bridge rectifiers and load voltage also satisfy (4) and (7).

4) *Mode 4:* $u_{s\_24}>0\&u_{s\_24}>u_{\mathrm{Load\_24}}$, in the interval of $\omega t \in [\pi/6 + \omega t_1 + 2k\pi, \pi/3 - \omega t_1 + 2k\pi)$.

Under this case, the diodes D_p, VD_1, and VD_4 are turned-ON. Similarly, based on the KVL, the voltages relations are as follows:

$$\begin{cases} u_{\mathrm{REC1\_36}} - (0.5 - \alpha_{\mathrm{m}})u_{\mathrm{p\_36}} = u_{\mathrm{s\_36}} = u_{\mathrm{Load\_36}} \\ u_{\mathrm{REC1\_36}} - u_{\mathrm{REC2\_36}} = u_{\mathrm{p\_36}} = \frac{u_{\mathrm{s\_36}}}{m} \\ u_{\mathrm{REC1\_36}} = u_{\mathrm{REC1\_24}}. \end{cases} \tag{10}$$

From (10), the voltages $u_{\mathrm{REC2\_36}}$ and $u_{\mathrm{Load\_36}}$ can be represented by the voltage $u_{\mathrm{REC1\_24}}$

$$\begin{cases} u_{\mathrm{REC2\_36}} = \frac{2m-1-2\alpha_{\mathrm{m}}}{2m+1-2\alpha_{\mathrm{m}}} u_{\mathrm{REC1\_24}} \\ u_{\mathrm{Load\_36}} = \frac{2m}{2m+1-2\alpha_{\mathrm{m}}} u_{\mathrm{REC1\_24}}. \end{cases} \tag{11}$$

In combination with the above analysis, under normal operation mode, the output voltages of the rectifiers REC1 and REC2 can be obtained: (12) shown at the bottom of the next page.

The load voltage of the 36-pulse rectifier is as follows: Equation (13) shown at the bottom of the next page.

From the viewpoint of minimizing the ripple factor of the load voltage, the interval length, amplitude, and terminal values of each mode should be, respectively, the same. Based on the piecewise function expressions (13), it can be obtained that

$$\begin{cases} \omega t_1 = \frac{\pi}{6} - 2\omega t_1 \\ \omega t_1 + 2\arctan\left(-2\alpha_{\mathrm{m}} \tan\frac{\pi}{12}\right) = 0 \\ \frac{2m}{2m+1-2\alpha_{\mathrm{m}}} = \sqrt{4\alpha_{\mathrm{m}}^2 \sin^2(\frac{\pi}{12}) + \cos^2(\frac{\pi}{12})}. \end{cases} \tag{14}$$

From (14), the radian $\omega\, t_1$, the optimum turns ratios α_{m}, and m can be determined

$$\begin{cases} \omega t_1 = \frac{\pi}{18} \\ \alpha_{\mathrm{m}} = \tan(\frac{\pi}{36})/2\tan(\frac{\pi}{12}) \approx 0.1633 \\ m = \frac{(2\alpha_{\mathrm{m}}-1)x}{2x-2} \approx 10.7460 \end{cases}$$

$$x = \sqrt{4\alpha_{\mathrm{m}}^2 \sin^2(\frac{\pi}{12}) + \cos^2(\frac{\pi}{12})}. \tag{15}$$

Therefore, the waveforms of the voltages $u_{\mathrm{REC1\_36}}$, $u_{\mathrm{REC2\_36}}$, and $u_{\mathrm{Load\_36}}$ can be plotted as shown in Fig. 3. The minimum value of the load voltage is 2.366*KE*.

III. Diode Open-Circuit Fault Analysis on the Parallel-Connected 36-Pulse Rectifier

Based on the location of the fault diode, this part divides the fault conditions into two types, the open-circuit fault diode in the main circuit and in the dc-side HRC are, respectively, discussed.

A. Single Diode Open-Circuit Fault in the Main Circuit

Among all kinds of diode open-circuit faults, the probability of the single diode open-circuit fault in the main circuit is quite

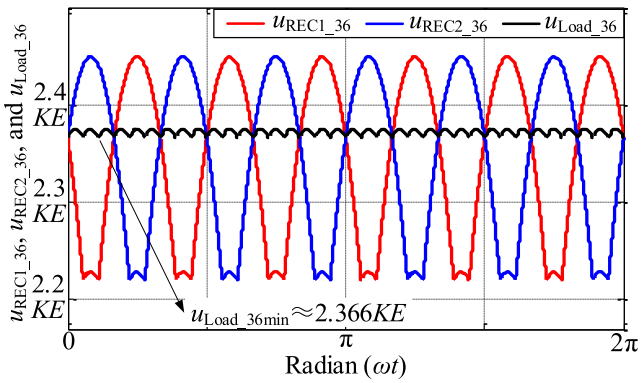

Fig. 3. Waveforms of voltages $u_{\mathrm{REC1\_36}}$, $u_{\mathrm{REC2\_36}}$, and $u_{\mathrm{Load\_36}}$.

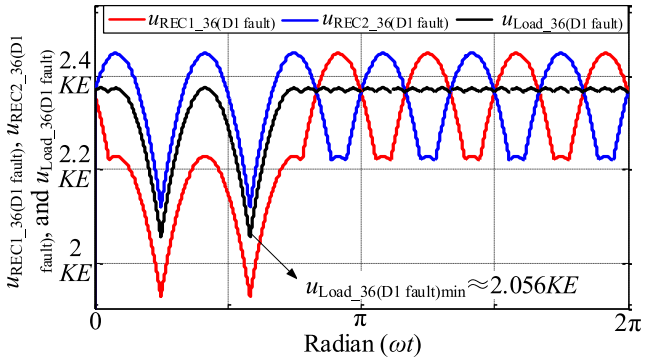

Fig. 4. Waveforms of voltages $u_{\mathrm{REC1\_36}(D1\ \mathrm{fault})}$, $u_{\mathrm{REC2\_36}(D1\ \mathrm{fault})}$, and $u_{\mathrm{Load\_36}(D1\ \mathrm{fault})}$.

high, so that it is the research emphasis and foundation. We take diode D_1 open-circuit fault as an example to study its operation modes and fault characteristics.

The normal conduction interval of diode D_1 is $\omega t \in [\pi/6 - \omega t_1, \pi/3 + \omega t_1] \cup [\pi/2 - \omega t_1, 2\pi/3 + \omega t_1]$. When the open-circuit fault occurs, the operation modes of the two three-phase rectifiers are changed, the rectifier REC1 is under the reverse voltage and turned-OFF; while the rectifier REC2 is operating in the six-pulse rectification state. In this fault interval, the diodes D_q, VD_2, and VD_3 in the dc-side HRC are turned-ON, so that the voltage relations fulfill that in *Mode2*. The affected intervals of voltages u_{REC1}, u_{REC2}, and u_{Load} are (unnumbered equation shown at the bottom of this page).

TABLE I
MINIMUM POINTS OF THE LOAD VOLTAGE UNDER EACH DIODE OPEN-CIRCUIT FAULT

Diode	D_1	D_2	D_3	D_4	D_5	D_6
Phase	$\frac{5\pi}{12}\pm\frac{\pi}{6}$	$\frac{17\pi}{12}\pm\frac{\pi}{6}$	$\frac{13\pi}{12}\pm\frac{\pi}{6}$	$\frac{7\pi}{12}\pm\frac{\pi}{6}$	$\frac{7\pi}{4}\pm\frac{\pi}{6}$	$\frac{3\pi}{4}\pm\frac{\pi}{6}$
Diode	D_1'	D_2'	D_3'	D_4'	D_5'	D_6'
Phase	$\frac{7\pi}{12}\pm\frac{\pi}{6}$	$\frac{19\pi}{12}\pm\frac{\pi}{6}$	$\frac{5\pi}{4}\pm\frac{\pi}{6}$	$\frac{\pi}{4}\pm\frac{\pi}{6}$	$\frac{23\pi}{12}\pm\frac{\pi}{6}$	$\frac{11\pi}{12}\pm\frac{\pi}{6}$

From (8) and (9), the expressions of $u_{\mathrm{REC1\_36}}$, $u_{\mathrm{REC2\_36}}$, and $u_{\mathrm{Load\_36}}$ in their corresponding affected intervals are shown in (16) and (17) shown at the bottom of the next page.

In combination with (16) and (17), the waveforms of $u_{\mathrm{REC1\_36(D1\ fault)}}$, $u_{\mathrm{REC2\_36(D1\ fault)}}$, and $u_{\mathrm{Load\_36(D1\ fault)}}$ under diode D_1 open-circuit fault can be plotted in Fig. 4. The voltage $u_{\mathrm{Load\_36}(D1\ \mathrm{fault})}$ takes the minimum value of around $2.056KE$ at the radians of $\pi/4$ and $7\pi/12$. Compared with normal operation mode, the maximum load voltage drop is $0.309KE$ under this fault condition. Similarly, the minimum points of the load voltage under each diode open-circuit fault are presented in Table I, which correspond to the midpoints of the conduction intervals under normal operation.

For this 36-pulse rectifier, based on the KVL, the load voltage cannot be affected by the load resistance. When the input voltage and the type of the phase-shifting transformer are determined, the load voltage waveform can be accordingly determined.

B. Single Diode Open-Circuit Fault in the DC Side Harmonic Reduction Circuit

Due to the use of dual passive HRC, the diode open-circuit fault in the double-tap IPR or in the single-phase rectifier cannot be ignored. We take diode D_p open-circuit fault (*Case1*) and

$$u_{\mathrm{REC1\_36}} = \begin{cases} \sqrt{6}KE\sin(\omega t + \frac{7\pi}{12} - \frac{k\pi}{3}) & \omega t \in \left[\frac{k\pi}{3}, \omega t_1 + \frac{k\pi}{3}\right) \\ \sqrt{6}KE\frac{2m-1-2\alpha_{\mathrm{m}}}{2m+1-2\alpha_{\mathrm{m}}}\sin(\omega t + \frac{5\pi}{12} - \frac{k\pi}{3}) & \omega t \in \left[\omega t_1 + \frac{k\pi}{3}, \frac{\pi}{6} - \omega t_1 + \frac{k\pi}{3}\right) \\ \sqrt{6}KE\sin(\omega t + \frac{\pi}{4} - \frac{k\pi}{3}) & \omega t \in \left[\frac{\pi}{6} - \omega t_1 + \frac{k\pi}{3}, \frac{(k+1)\pi}{3}\right) \end{cases} \quad u_{\mathrm{REC2\_36}}$$

$$= \begin{cases} \sqrt{6}KE\sin(\omega t + \frac{5\pi}{12} - \frac{k\pi}{3}) & \omega t \in \left[\frac{k\pi}{3}, \frac{\pi}{6} + \omega t_1 + \frac{k\pi}{3}\right) \\ \sqrt{6}KE\frac{2m-1-2\alpha_{\mathrm{m}}}{2m+1-2\alpha_{\mathrm{m}}}\sin(\omega t + \frac{\pi}{4} - \frac{k\pi}{3}) & \omega t \in \left[\frac{\pi}{6} + \omega t_1 + \frac{k\pi}{3}, \frac{\pi}{3} - \omega t_1 + \frac{k\pi}{3}\right) \\ \sqrt{6}KE\sin(\omega t + \frac{\pi}{12} - \frac{k\pi}{3}) & \omega t \in \left[\frac{\pi}{3} - \omega t_1 + \frac{k\pi}{3}, \frac{(k+1)\pi}{3}\right) \end{cases} \tag{12}$$

$$u_{\mathrm{Load\_36}} = \begin{cases} A_{\mathrm{m}}\sin\left[\omega t + \frac{\pi}{2} + \arctan(-2\alpha_{\mathrm{m}}\tan\frac{\pi}{12}) - \frac{k\pi}{6}\right] & \omega t \in \left[\frac{k\pi}{6}, \omega t_1 + \frac{k\pi}{6}\right) \\ \sqrt{6}KE\frac{2m}{2m+1-2\alpha_{\mathrm{m}}}\sin(\omega t + \frac{5\pi}{12} - \frac{k\pi}{6}) & \omega t \in \left[\omega t_1 + \frac{k\pi}{6}, -\omega t_1 + \frac{(k+1)\pi}{6}\right) \\ A_{\mathrm{m}}\sin\left[\omega t + \frac{\pi}{3} + \arctan(2\alpha_{\mathrm{m}}\tan\frac{\pi}{12}) - \frac{k\pi}{6}\right] & \omega t \in \left[-\omega t_1 + \frac{(k+1)\pi}{6}, \frac{(k+1)\pi}{6}\right) \end{cases}$$

$$A_{\mathrm{m}} = \sqrt{6}KE\sqrt{\cos^2(\frac{\pi}{12}) + 4\alpha_{\mathrm{m}}^2\sin^2(\frac{\pi}{12})} \tag{13}$$

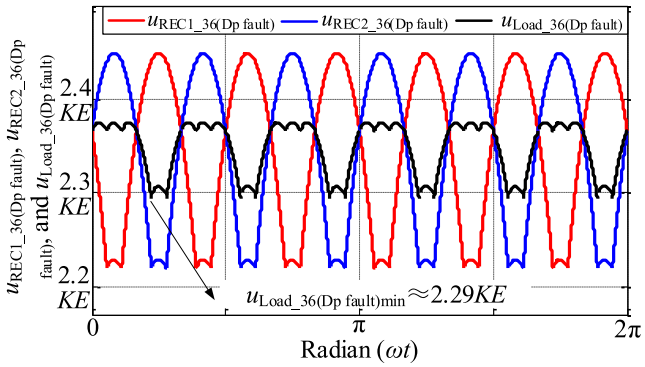

Fig. 5. Waveforms of voltages $u_{\mathrm{REC1\_36}(Dp\ \mathrm{fault})}$, $u_{\mathrm{REC2\_36}(Dp\ \mathrm{fault})}$, and $u_{\mathrm{Load\_36}(Dp\ \mathrm{fault})}$.

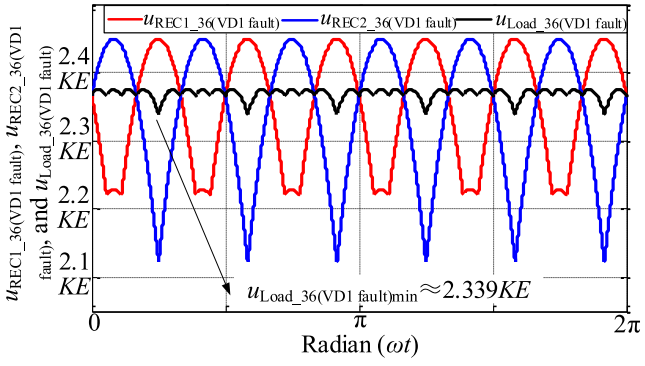

Fig. 6. Waveforms of voltages $u_{\mathrm{REC1\_36}\ (VD1\ \mathrm{fault})}$, $u_{\mathrm{REC2\_36}\ (VD1\ \mathrm{fault})}$, and $u_{\mathrm{Load\_36}\ (VD1\ \mathrm{fault})}$.

diode VD_1 open-circuit fault (*Case2*) as examples to study their fault characteristics.

1) Case1: Diode $\mathrm{D_p}$ *Open-Circuit Fault:* Under this case, the originally conduction intervals of diode D_q is unaffected, but due to the diode D_p is open-circuit, the diode D_q is continuously conducting all the time. Although the operation modes of rectifiers REC1 and REC2 are not changed, according to the KVL, the load voltage u_{Load} has to change.

When the single-phase rectifier is turned-OFF, the load voltage $u_{\mathrm{Load\_36}}$ is changed into

$$u_{\mathrm{Load\_36(Dpfault)}} = u_{\mathrm{REC1\_24}} - (0.5+\alpha_{\mathrm{m}})u_{\mathrm{p\_24}}. \tag{18}$$

When the diodes VD_1 and VD_4 in the single-phase rectifier are turned-ON, the voltage relations are changed into

$$\begin{cases} u_{\mathrm{REC1\_36}} - (0.5-\alpha_{\mathrm{m}})u_{\mathrm{p\_36}} = u_{\mathrm{s\_36}} = u_{\mathrm{Load\_36}} \\ u_{\mathrm{REC1\_36}} - u_{\mathrm{REC2\_36}} = u_{\mathrm{p\_36}} = \frac{u_{\mathrm{s\_36}}}{m} \\ u_{\mathrm{REC1\_36}} = u_{\mathrm{REC1\_24}}. \end{cases} \tag{19}$$

From (19), the load voltage can be obtained as follows:

$$u_{\mathrm{Load\_36(Dpfault)}} = \frac{2m}{2m+2\alpha_{\mathrm{m}}+1} u_{\mathrm{REC1\_24}}. \tag{20}$$

When the diodes VD_2 and VD_3 in the single-phase rectifier are turned-ON, the voltage relations are consistent with (8) and (9).

Based on the above analysis, the load voltage can be obtained as follows. Equation (21) shown at the bottom of the next page.

Substitute (15) into (21), the waveforms of $u_{\mathrm{REC1\_36}(Dp\ \mathrm{fault})}$, $u_{\mathrm{REC2\_36}(Dp\ \mathrm{fault})}$, and $u_{\mathrm{Load\_36}(Dp\ \mathrm{fault})}$ can be plotted as shown in Fig. 5.

From Fig. 5, the minimum value of the load voltage is $2.29KE$ at the radians of $2\pi/9+k\pi/3$ and $5\pi/18+k\pi/3$. Similarly, when the open-circuit fault occurs in diode D_q, the load voltage takes the minimum value at $7\pi/18+k\pi/3$ and $4\pi/9+k\pi/3$.

2) Case2: Diode VD_1 *Open-Circuit Fault:* Due to the pulse number increases of voltages u_{REC1} and u_{REC2} is the effect of the single-phase rectifier, when open-circuit fault occurs on one or two diodes of VD_1 and VD_4, the operation mode of rectifier REC1 is not changed, but the rectifier REC2 is operating under the six-pulse rectification state.

Therefore, the expression of voltage u_{REC1} is consistent with that shown in (12), and voltage u_{REC2} is changed into (22) shown at the bottom of the next page.

In combination with (7), (12), (13), and (22), the expression of load voltage $u_{\mathrm{Load\_36}(VD1\ \mathrm{fault})}$ can be obtained (23) shown at the bottom of the next page.

Based on (22) and (23), the waveforms of voltages $u_{\mathrm{REC1\_36}(VD1\ \mathrm{fault})}$, $u_{\mathrm{REC2\_36}(VD1\ \mathrm{fault})}$ and $u_{\mathrm{Load\_36}(VD1\ \mathrm{fault})}$ can be plotted as shown in Fig. 6.

$$\begin{cases} u_{\mathrm{REC1}}, u_{\mathrm{Load}} : \omega t \in [\pi/6-\omega t_1, \pi/3+\omega t_1] \cup [\pi/2-\omega t_1, 2\pi/3+\omega t_1] \\ u_{\mathrm{REC2}} : \omega t \in [\pi/6+\omega t_1, \pi/3-\omega t_1] \cup [\pi/2+\omega t_1, 2\pi/3-\omega t_1] \end{cases}$$

$$u_{\mathrm{REC2\_36(D1fault)}} = \begin{cases} \sqrt{6}KE\sin(\omega t+\frac{5\pi}{12}) \omega t \in \left[\frac{\pi}{6}+\omega t_1, \frac{\pi}{4}\right) \\ \sqrt{6}KE\sin(\omega t+\frac{\pi}{12}) \omega t \in \left[\frac{\pi}{4}, \frac{\pi}{3}-\omega t_1\right] \cup \left[\frac{\pi}{2}+\omega t_1, \frac{7\pi}{12}\right) \\ \sqrt{6}KE\sin(\omega t-\frac{\pi}{4}) \omega t \in \left[\frac{7\pi}{12}, \frac{2\pi}{3}-\omega t_1\right] \end{cases} \quad u_{\mathrm{REC1\_36(D1fault)}}$$

$$= \begin{cases} \frac{2m-1-2\alpha_{\mathrm{m}}}{2m+1-2\alpha_{\mathrm{m}}}\sqrt{6}KE\sin(\omega t+\frac{5\pi}{12}) \omega t \in \left[\frac{\pi}{6}-\omega t_1, \frac{\pi}{4}\right) \\ \frac{2m-1-2\alpha_{\mathrm{m}}}{2m+1-2\alpha_{\mathrm{m}}}\sqrt{6}KE\sin(\omega t+\frac{\pi}{12}) \omega t \in \left[\frac{\pi}{4}, \frac{\pi}{3}+\omega t_1\right] \cup \left[\frac{\pi}{2}-\omega t_1, \frac{7\pi}{12}\right) \\ \frac{2m-1-2\alpha_{\mathrm{m}}}{2m+1-2\alpha_{\mathrm{m}}}\sqrt{6}KE\sin(\omega t-\frac{\pi}{4}) \omega t \in \left[\frac{7\pi}{12}, \frac{2\pi}{3}+\omega t_1\right] \end{cases} \tag{16}$$

$$u_{\mathrm{Load\_36(D1fault)}} = \begin{cases} \frac{2m}{2m+1-2\alpha_{\mathrm{m}}}\sqrt{6}KE\sin(\omega t+\frac{5\pi}{12}) \omega t \in \left[\frac{\pi}{6}-\omega t_1, \frac{\pi}{4}\right) \\ \frac{2m}{2m+1-2\alpha_{\mathrm{m}}}\sqrt{6}KE\sin(\omega t+\frac{\pi}{12}) \omega t \in \left[\frac{\pi}{4}, \frac{\pi}{3}+\omega t_1\right] \cup \left[\frac{\pi}{2}-\omega t_1, \frac{7\pi}{12}\right) \\ \frac{2m}{2m+1-2\alpha_{\mathrm{m}}}\sqrt{6}KE\sin(\omega t-\frac{\pi}{4}) \omega t \in \left[\frac{7\pi}{12}, \frac{2\pi}{3}+\omega t_1\right] \end{cases} \tag{17}$$

TABLE II
POWER QUALITY OF THE TWO MPRS WITH SINGLE/DUAL PASSIVE HRC

Topology	Condition	THD of $i_{a(Normal)}$	THD of $i_{a(D1\_fault)}$	THD of $i_{a(Dp\_fault)}$	THD of $i_{a(VD1\_fault)}$	Minimum voltage of $u_{Load(Normal)}$	Minimum voltage of $u_{Load(D1\_fault)}$	Minimum voltage of $u_{Load(Dp\_fault)}$	Minimum voltage of $u_{Load(VD1\_fault)}$
24-pulse rectifier	Theory	7.28%	15.45%	/	11.65%	2.346*KE*	2.049*KE*	/	2.285*KE*
	Experiment *E*=50V	4.74%	21.03%	/	7.97%	103V	92V	/	99.8V
36-pulse rectifier	Theory	5.04%	14.72%	10.89%	6.67%	2.366*KE*	2.056*KE*	2.29*KE*	2.339*KE*
	Experiment *E*=50V	3.62%	17.36%	5.05%	5.31%	102V	91V	99.2V	100V

From Fig. 6, the minimum value of the load voltage is 2.339*KE* at the radians of $\pi/4+k\pi/3$. Similarly, when the open-circuit fault occurs in diode VD_2 or VD_3, the load voltage takes the minimum value at $\pi/12+k\pi/3$.

IV. SIMULATION AND EXPERIMENTAL VERIFICATION

Based on Fig. 1, the simulation model and experiment platform are constructed, the phase-shifting transformer is the *Y*-connected autotransformer with the step-up ratio (*K*) of $(3-\sqrt{3})/\sqrt{2}$; the turns ratios of the IPR are 0.163(α_m) and 10.75(*m*), respectively; the rms value of the input voltage is 50 V; and the load resistance is 30 Ω.

First, the experimental results under normal operation state are presented in Fig. 7, which can provide references.

Fig. 8 shows the verification results under the single diode D_1 open-circuit fault in the main circuit. The affected interval of the three-phase input currents is consistent with the normal conduction interval of diode D_1, the rest intervals are not affected [Fig. 8(a) and (c)]. In experiment, the THD value of the input current $i_{a\_36(D1\ fault)}$ is reduced from 3.62% to 17.36% as presented in Fig. 8(d), the lower order harmonics, such as the second, fourth, and fifth, appear under fault condition. Fig. 8(e) gives the output voltages of the rectifiers REC1 and REC2, which are consistent with the theoretical analysis. From Fig. 8(b) and (f), the minimum value of the load voltage is ∼91 V in simulation and experiment, which are slightly lower than theoretical value (92.167 V) due to the actual voltage drops on diodes and lines. Besides, Fig. 8(f) also presents the relations between the fault diode and phases of the minimum load voltages, the results satisfy that shown in Table I.

Similarly, the verifications of diode open-circuit faults in the dc-side HRC are also performed. Figs. 9 and 10 are the results under diode D_p and VD_1 open-circuit fault, respectively. Compared with the main circuit diode D_1 open-circuit fault, as can be observed from Figs. 9(a), (c) and 10(a), (c), the current waveforms under these two faults are more symmetrical. The THD values of the input currents $i_{a1\_36(Dp\ fault)}$ and $i_{a1\_36(VD1\ fault)}$ are 5.05% and 5.31%, respectively.

Fig. 9(e) and (f) are output currents of the phase-shifting transformer, the operation modes of the main circuit do not change under the diode D_p fault condition, so that the output voltages of REC1 and REC2 are same with the normal operation state [see Fig. 9(g)]. Fig. 9(b) and (h) presents verification results

$$u_{\mathrm{Load\_36(Dpfault)}}=\begin{cases} A_{\mathrm{m}}\sin\left[\omega t+\frac{\pi}{2}+\arctan(-2\alpha_{\mathrm{m}}\tan\frac{\pi}{12})-\frac{k\pi}{3}\right] & \omega t\in\left[\frac{k\pi}{3},\omega t_1+\frac{k\pi}{3}\right) \\ \sqrt{6}KE\frac{2m}{2m+1-2\alpha_{\mathrm{m}}}\sin(\omega t+\frac{5\pi}{12}-\frac{k\pi}{3}) & \omega t\in\left[\omega t_1+\frac{k\pi}{3},-\omega t_1+\frac{(2k+1)\pi}{6}\right) \\ A_{\mathrm{m}}\sin\left[\omega t+\frac{\pi}{3}+\arctan(2\alpha_{\mathrm{m}}\tan\frac{\pi}{12})-\frac{k\pi}{3}\right] & \omega t\in\left[-\omega t_1+\frac{(2k+1)\pi}{6},\omega t_1+\frac{(2k+1)\pi}{6}\right) \\ \sqrt{6}KE\frac{2m}{2m+2\alpha_{\mathrm{m}}+1}\sin(\omega t+\frac{\pi}{4}-\frac{k\pi}{3}) & \omega t\in\left[\omega t_1+\frac{(2k+1)\pi}{6},-\omega t_1+\frac{(k+1)\pi}{3}\right) \\ A_{\mathrm{m}}\sin\left[\omega t+\frac{\pi}{6}+\arctan(-2\alpha_{\mathrm{m}}\tan\frac{\pi}{12})-\frac{k\pi}{3}\right] & \omega t\in\left[-\omega t_1+\frac{(k+1)\pi}{3},\frac{(k+1)\pi}{3}\right) \end{cases}$$

$$A_{\mathrm{m}}=\sqrt{6}KE\sqrt{\cos^2(\frac{\pi}{12})+4\alpha_{\mathrm{m}}^2\sin^2(\frac{\pi}{12})} \tag{21}$$

$$u_{\mathrm{REC2\_36(VD1fault)}}=\begin{cases} \sqrt{6}KE\sin(\omega t+\frac{5\pi}{12}-\frac{k\pi}{3})\omega t\in\left[\frac{k\pi}{3},\frac{\pi}{4}+\frac{k\pi}{3}\right) \\ \sqrt{6}KE\sin(\omega t+\frac{\pi}{12}-\frac{k\pi}{3})\omega t\in\left[\frac{\pi}{4}+\frac{k\pi}{3},\frac{(k+1)\pi}{3}\right) \end{cases} \tag{22}$$

$$u_{\mathrm{Load\_36(VD1fault)}}=\begin{cases} A_{\mathrm{m}}\sin\left[\omega t+\frac{\pi}{2}+\arctan(-2\alpha_{\mathrm{m}}\tan\frac{\pi}{12})-\frac{k\pi}{3}\right] & \omega t\in\left[\frac{k\pi}{3},\omega t_1+\frac{k\pi}{3}\right) \\ \sqrt{6}KE\frac{2m}{2m+1-2\alpha_{\mathrm{m}}}\sin(\omega t+\frac{5\pi}{12}-\frac{k\pi}{3}) & \omega t\in\left[\omega t_1+\frac{k\pi}{3},-\omega t_1+\frac{\pi}{6}+\frac{k\pi}{3}\right) \\ A_{\mathrm{m}}\sin\left[\omega t+\frac{\pi}{3}+\arctan(2\alpha_{\mathrm{m}}\tan\frac{\pi}{12})-\frac{k\pi}{3}\right] & \omega t\in\left[-\omega t_1+\frac{\pi}{6}+\frac{k\pi}{3},\frac{\pi}{6}+\frac{k\pi}{3}\right) \\ A_{\mathrm{m}}\sin\left[\omega t+\frac{\pi}{3}+\arctan(-2\alpha_{\mathrm{m}}\tan\frac{\pi}{12})-\frac{k\pi}{3}\right] & \omega t\in\left[\frac{\pi}{6}+\frac{k\pi}{3},\frac{\pi}{4}+\frac{k\pi}{3}\right) \\ A_{\mathrm{m}}\sin\left[\omega t+\frac{\pi}{6}+\arctan(2\alpha_{\mathrm{m}}\tan\frac{\pi}{12})-\frac{k\pi}{3}\right] & \omega t\in\left[\frac{\pi}{4}+\frac{k\pi}{3},\frac{(k+1)\pi}{3}\right) \end{cases}$$

$$A_{\mathrm{m}}=\sqrt{6}KE\sqrt{\cos^2(\frac{\pi}{12})+4\alpha_{\mathrm{m}}^2\sin^2(\frac{\pi}{12})} \tag{23}$$

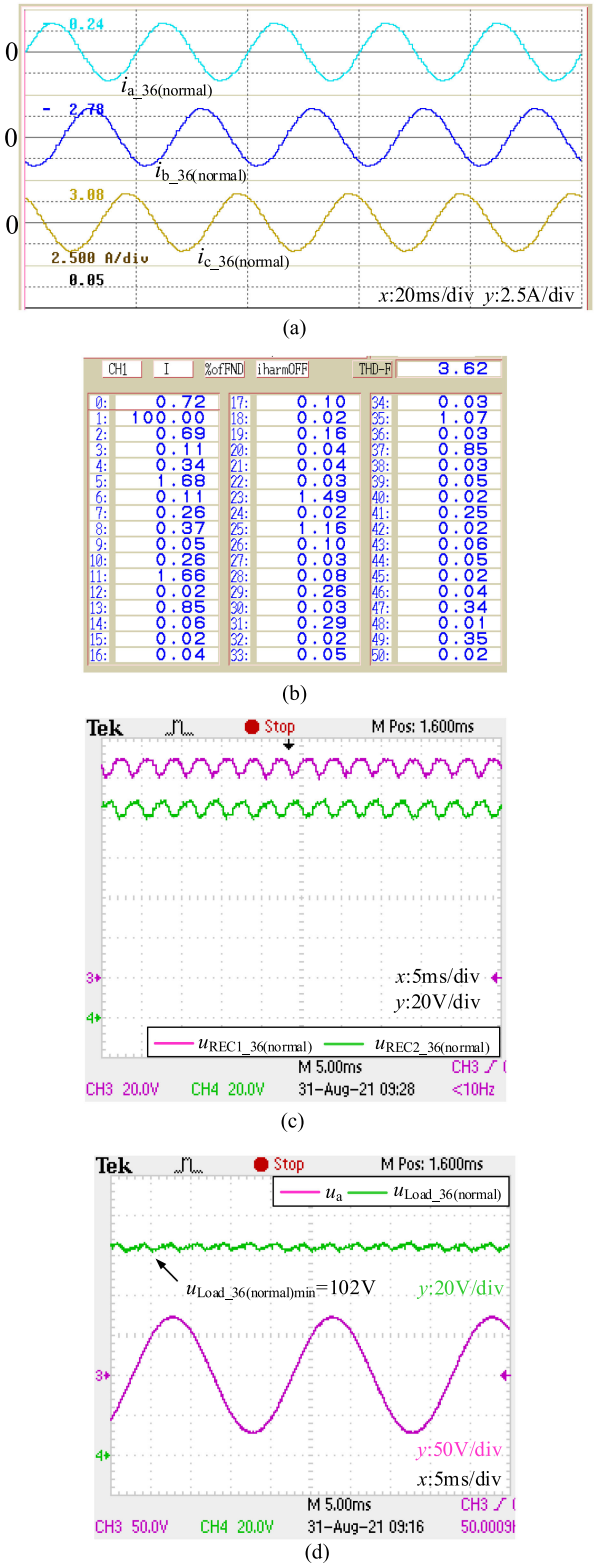

Fig. 7. Verification results under normal operation. (a) Experimental result of the input currents $i_{a\_36(normal)}$, $i_{b\_36(normal)}$, and $i_{c\_36(normal)}$. (b) Spectrum of the input current $i_{a\_36(normal)}$. (c) Experimental result of voltages $u_{REC1\_36(normal)}$ and $u_{REC2\_36(normal)}$. (d) Experimental result of voltage $u_{Load\_36(normal)}$.

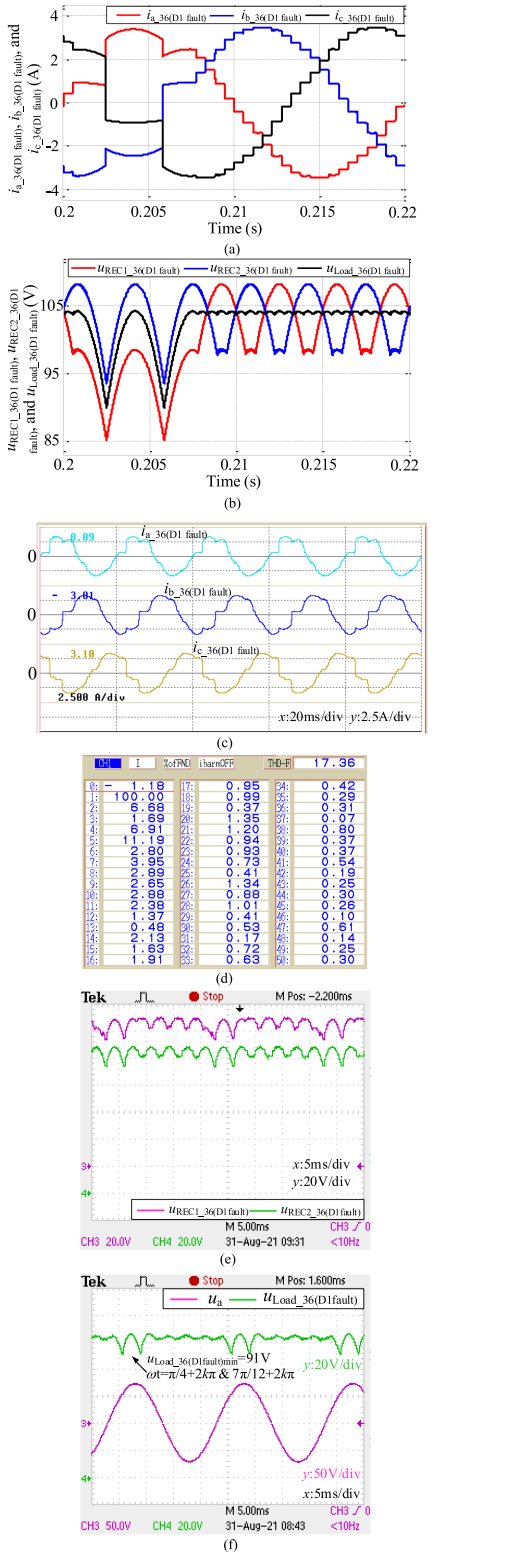

Fig. 8. Verification results under diode D_1 open-circuit fault. (a) Simulation result of the input currents $i_{a\_36(D1\ fault)}$, $i_{b\_36(D1\ fault)}$, and $i_{c\_36(D1\ fault)}$. (b) Simulation result of voltages $u_{REC1\_36(D1\ fault)}$, $u_{REC2\_36(D1\ fault)}$, and $u_{Load\_36(D1\ fault)}$. (c) Experimental result of the input currents $i_{a\_36(D1\ fault)}$, $i_{b\_36(D1\ fault)}$, and $i_{c\_36(D1\ fault)}$. (d) Spectrum of the input current $i_{a\_36(D1\ fault)}$. (e) Experimental result of voltages $u_{REC1\_36(D1\ fault)}$ and $u_{REC2\_36(D1\ fault)}$. (f) Experimental result of voltage $u_{Load\_36(D1\ fault)}$.

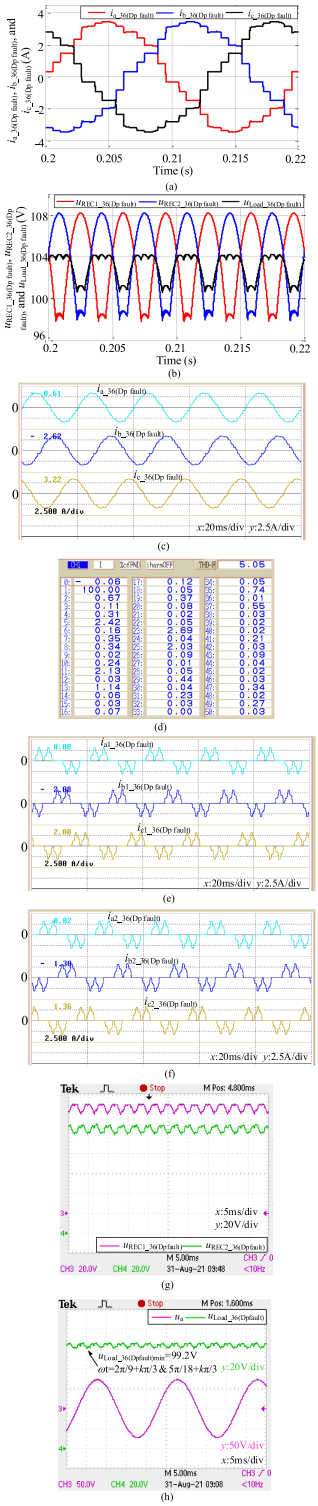

Fig. 9. Verification results under diode D_p open-circuit fault. (a) Simulation result of the input currents $i_{\mathrm{a\_36}(Dp\ \mathrm{fault})}$, $i_{\mathrm{b\_36}(Dp\ \mathrm{fault})}$, and $i_{\mathrm{c\_36}(Dp\ \mathrm{fault})}$. (b) Simulation result of voltages $u_{\mathrm{REC1\_36}(Dp\ \mathrm{fault})}$, $u_{\mathrm{REC2\_36}(Dp\ \mathrm{fault})}$, and $u_{\mathrm{Load\_36}(Dp\ \mathrm{fault})}$. (c) Experimental result of the input currents $i_{\mathrm{a\_36}(Dp\ \mathrm{fault})}$, $i_{\mathrm{b\_36}(Dp\ \mathrm{fault})}$, and $i_{\mathrm{c\_36}(Dp\ \mathrm{fault})}$. (d) Spectrum of the input current $i_{\mathrm{a\_36}(Dp\ \mathrm{fault})}$. (e) Experimental result of the currents $i_{\mathrm{a1\_36}(Dp\ \mathrm{fault})}$, $i_{\mathrm{b1\_36}(Dp\ \mathrm{fault})}$, and $i_{\mathrm{c1\_36}(Dp\ \mathrm{fault})}$. (f) Experimental result of the currents $i_{\mathrm{a2\_36}(Dp\ \mathrm{fault})}$, $i_{\mathrm{b2\_36}(Dp\ \mathrm{fault})}$, and $i_{\mathrm{c2\_36}(Dp\ \mathrm{fault})}$. (g) Experimental result of voltages $u_{\mathrm{REC1\_36}(Dp\ \mathrm{fault})}$ and $u_{\mathrm{REC2\_36}(Dp\ \mathrm{fault})}$. (h) Experimental result of voltage $u_{\mathrm{Load\_36}(Dp\ \mathrm{fault})}$.

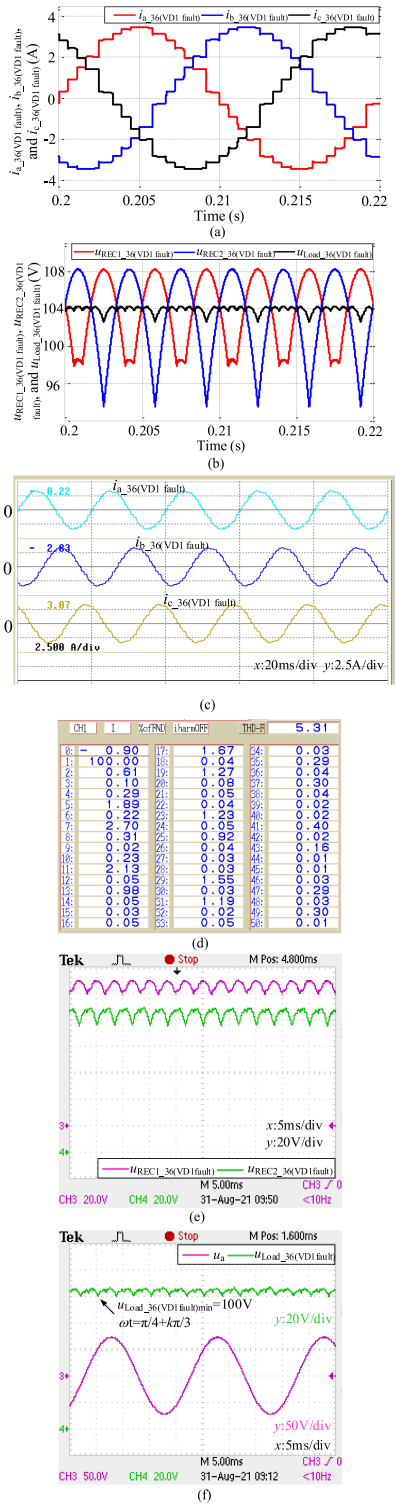

Fig. 10. Verification results under diode VD_1 open-circuit fault. (a) Simulation result of the input currents $i_{\mathrm{a\_36}(VD1\ \mathrm{fault})}$, $i_{\mathrm{b\_36}(VD1\ \mathrm{fault})}$, and $i_{\mathrm{c\_36}(VD1\ \mathrm{fault})}$. (b) Simulation result of voltages $u_{\mathrm{REC1\_36}(VD1\ \mathrm{fault})}$, $u_{\mathrm{REC2\_36}(VD1\ \mathrm{fault})}$, and $u_{\mathrm{Load\_36}(VD1\ \mathrm{fault})}$. (c) Experimental result of the input currents $i_{\mathrm{a\_36}(VD1\ \mathrm{fault})}$, $i_{\mathrm{b\_36}(VD1\ \mathrm{fault})}$, and $i_{\mathrm{c\_36}(VD1\ \mathrm{fault})}$. (d) Spectrum of the input current $i_{\mathrm{a\_36}(VD1\ \mathrm{fault})}$. (e) Experimental result of voltages $u_{\mathrm{REC1\_36}(VD1\ \mathrm{fault})}$ and $u_{\mathrm{REC2\_36}(VD1\ \mathrm{fault})}$. (f) Experimental result of voltage $u_{\mathrm{Load\_36}(VD1\ \mathrm{fault})}$.

of voltages $u_{\mathrm{Load\_36}(Dp\ \mathrm{fault})}$, the minimum value of the load voltage is 100.8 V in simulation and 99.2 V in experiment, which are consistent with theoretical calculation, and the corresponding phases are $2\pi/9+k\pi/3$ and $5\pi/18+k\pi/3$.

Fig. 10(b) shows the simulation result of the voltages $u_{\mathrm{REC1\_36}}$ ($VD1$ fault), $u_{\mathrm{REC2\_36}}$ ($VD1$ fault), and $u_{\mathrm{Load\_36}}$ ($VD1$ fault), it can be clearly observed that the rectifier REC2 is under the six-pulse rectification state, and the operation state of the rectifier REC1 is not affected. The experimental results [see Figs. 9(f) and 10(e)] are consistent with the simulations, the minimum value of the load voltage is ∼100 V at the phases of $\pi/4+k\pi/3$.

Table II presents the power quality comparisons between the 24-pulse rectifier with single passive HRC [16] and the 36-pulse rectifier with dual passive HRC discussed in this article. In [16], the main topology of the MPR consists with that in Fig. 1, the HRC is formed by an IPR and a single-phase diode bridge rectifier. Except for the HRC, the other conditions remain the same between these two MPRs.

In combination with Table II, the following conclusions can be obtained.

1) There are some common points presented in these two MPRs, compared with the diode open-circuit fault in the main circuit, the fault in the HRC causes less damage on the power quality.
2) Compared with the currents, the load voltages have more obvious fault characteristics; in the 36-pulse rectifier, the fault types can also be determined on the basis of the load voltage waveforms.
3) Under diode open-circuit fault conditions, the use of dual passive HRC can slightly reduce the THD value of the ac side input current, but the load voltage drop is approximately the same in these two MPRs.

V. Conclusion

Based on the normal operation mode of the 36-pulse rectifier, this article discussed the operation modes under the diode open-circuit fault both in the main circuit and in the dc-side HRC. In combination with theoretical derivations and experimental verifications, the waveform of load voltage can directly reflect the location of the fault diode, and the corresponding relations between the fault characteristic and fault diode have been established. When the diode open-circuit fault occurs in the HRC, compared with the main circuit diode open-circuit fault, the power quality can be maintained in a better state. From the comparisons between the MPRs with single/dual passive HRC, although the increase of diodes in dual passive HRC may increase the failure probability, the ac side power quality under the fault states can be improved with the power quality improvement under the steady state. Therefore, the use of dual passive HRC is a reliable method to improve the power quality of MPRs.

The study of fault characteristics is an important basis for the future design of fault diagnosis system. According to the theoretical waveforms, the fault diagnosis system should have the function of detecting the minimum load voltage and the corresponding phase of the minimum point, so as to determine the position of the faulty diode. The above research is useful for the fault detection of the 36-pulse rectifier and the design of new MPRs.

References

[1] Q. Du, L. Gao, Q. Li, T. Li, and F. Meng, "Harmonic reduction methods at DC side of parallel-connected multipulse rectifiers: A review," *IEEE Trans. Power Electron.*, vol. 36, no. 3, pp. 2768–2782, Mar. 2021.

[2] B. Singh, G. Bhuvaneswari, and V. Garg, "An improved power-quality 30-pulse AC–DC for varying loads," *IEEE Trans. Power Del.*, vol. 22, no. 2, pp. 1179–1187, Apr. 2007.

[3] B. Singh, G. Bhuvaneswari, V. Garg, and A. Chandra, "Star connected autotransformer based 30-pulse AC-DC converter for power quality improvement in vector controlled induction motor drives," in *Proc. IEEE Power India Conf.*, 2006, pp. 1–6.

[4] J. Chen, Y. Shen, J. Chen, H. Bai, C. Gong, and F. Wang, "Evaluation on the autoconfigured multipulse AC/DC rectifiers and their application in more electric aircrafts," *IEEE Trans. Transp. Electron.*, vol. 6, no. 4, pp. 1721–1739, Dec. 2020.

[5] S. Yang, F. Meng, and W. Yang, "Optimum design of interphase reactor with double-tap changer applied to multipulse diode rectifier," *IEEE Trans. Ind. Electron.*, vol. 57, no. 9, pp. 3022–3029, Sep. 2010.

[6] F. Meng, X. Xu, and L. Gao, "A simple harmonic reduction method in multipulse rectifier using passive devices," *IEEE Trans. Ind. Informat.*, vol. 13, no. 5, pp. 2680–2692, Oct. 2017.

[7] Y. Lian, S. Yang, K. Xu, Y. Li, and W. Yang, "Harmonic reduction mechanism at DC link of two different 24-pulse rectifiers," in *Proc. IEEE Transp. Electrific. Conf. Expo.*, 2017, pp. 1–6.

[8] F. J. Chivite-Zabalza, A. J. Forsyth, and D. R. Trainer, "A simple, passive 24-pulse AC–DC converter with inherent load balancing," *IEEE Trans. Power Electron.*, vol. 21, no. 2, pp. 430–439, Mar. 2006.

[9] Y. Li, K. Xu, Y. Lian, W. Yang, and S. Yang, "A novel 36-pulse rectifier with a low loss interphase converter at DC side," in *Proc. IEEE Transp. Electrific. Conf. Expo.*, 2017, pp. 2–7.

[10] L. Gao, X. Xu, Z. Man, and J. Lee, "A 36-pulse diode-bridge rectifier using dual passive harmonic reduction methods at DC link," *IEEE Trans. Power Electron.*, vol. 34, no. 2, pp. 1216–1226, Feb. 2019.

[11] F. J. Chivite-Zabalza and A. J. Forsyth, "A passive 36-pulse AC–DC converter with inherent load balancing using combined harmonic voltage and current injection," *IEEE Trans. Power Electron.*, vol. 22, no. 3, pp. 1027–1035, May 2007.

[12] X. Lian, S. Yang, and W. Yang, "Optimum design of 48-pulse rectifier using unconventional interphase reactor," *IEEE Access*, vol. 7, pp. 61240–61250, 2019.

[13] F. Meng, W. Yang, S. Yang, and L. Gao, "Active harmonic reduction for 12-pulse diode bridge rectifier at DC side with two-stage auxiliary circuit," *IEEE Trans. Ind. Informat.*, vol. 11, no. 1, pp. 64–73, Feb. 2015.

[14] F. Meng, L. Gao, S. Yang, and W. Yang, "Effect of single-phasing on multipulse rectifier with active interphase reactor," *IEEE Trans. Power Electron.*, vol. 30, no. 5, pp. 2549–2555, May 2015.

[15] J. S. Perisé, M. Bakkar, and S. B. Rodríguez, "Open-circuit fault diagnosis and maintenance in multi-pulse parallel and series TRU topologies," *IEEE Trans. Power Electron.*, vol. 35, no. 10, pp. 10906–10916, Oct. 2020.

[16] Q. Du, L. Gao, W. Liu, X. Yin, and F. Meng, "Diode open-circuit fault research on the parallel-connected 24-pulse rectifier with DC-side passive harmonic reduction circuit," *IEEE Trans. Power Electron.*, vol. 37, no. 1, pp. 485–497, Jan. 2022.

Qingxiao Du was born in Shandong, China, in 1995. She received the B.S. degree in electrical engineering from the Harbin Institute of Technology, Weihai, China, in 2017, and the M.S. degree in electrical power engineering from the University of Southampton, Southampton, U.K., in 2018. She is currently working toward the Ph.D. degree in electrical engineering with the Harbin Institute of Technology, Weihai, China.

Her research interests include harmonic elimination and fault analysis of high-power rectifiers.

Lei Gao was born in Hebei, China, in 1982. She received the B.S., M.S., and Ph.D. degrees in electrical engineering from the Harbin Institute of Technology, Harbin, China, in 2005, 2007, and 2012, respectively.

Since 2012, she has been working as an Assistant Professor with the Harbin Institute of Technology, Weihai, China. Her research interests include power electronics and motor drives.

Quanhui Li was born in Shandong, China, in 1996. He received the B.S. and M.S. degrees in electrical engineering in 2018 and 2020, respectively, from the Harbin Institute of Technology, Weihai, China, where he is currently working toward the Ph.D. degree in electrical engineering.

His research interests include multipulse rectifier and high-power rectification.

Xinyu Yin was born in Shandong, China, in 1997. She received the B.S. degree in electrical engineering from Shandong Agricultural University, Tai'an, China, in 2020. She is currently working toward the M.S. degree in power electronics and power drives with the Harbin Institute of Technology, Weihai, China.

Her research interests include power electronic transformer and multiple power supply system.

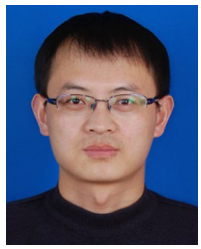

Fangang Meng (Member, IEEE) was born in Shandong, China, in 1982. He received the B.S. degree in thermal energy and power engineering, and the M.S. and Ph.D. degrees in electrical engineering from the Harbin Institute of Technology, Harbin, China, in 2005, 2007, and 2011, respectively.

Since 2020, he has been working as a Professor with the Harbin Institute of Technology, Weihai, China. His research interests include harmonic detection, stability analysis of converter, and high-power rectification.